A General Analytical Tool for the Design of Vibration Energy Harvesters (VEHs) Based on the Mechanical Impedance Concept

Dimitri Galayko and Philippe Basset

***Abstract*—This paper reports on a new approach for the analysis and design of vibration-to-electricity converters [vibration energy harvesters (VEHs)] operating in the mode of strong electromechanical coupling. The underlying concept is that the mechanical impedance is defined for a nonlinear electromechanical transducer on the basis of an equivalence between electrical and mechanical systems. This paper demonstrates how the mechanical impedance of the transducer depends not only on the geometry and the nature of the electromechanical transducer itself but also on the topology and on the operation mode of the conditioning circuit. The analysis is developed for resonant harvesters and is based on the first-harmonic method. It is applied to three electrostatic harvesters using an identical conditioning circuit but employing transducers with different geometries. For each of the three configurations, the mechanical impedance of the transducer is calculated and then used to determine the optimal electrical operation mode of the conditioning circuit, allowing a desired amplitude of the mobile-mass vibration to be obtained. This paper highlights how the parameters of the conditioning circuit and of the transducer impact the transducer's mechanical impedance, directly affecting the impedance matching between the energy source (resonator) and the transducer. This technique permits the design of highly efficient VEHs whatever the means of transduction.**

***Index Terms*—Electrostatic transducer, first-harmonic method, mechanical impedance, mechanical impedance matching, vibration energy harvester (VEH).**

I. Introduction

A. Objectives of This Study

VIBRATION energy harvesters (VEHs) convert the energy of ambient mechanical vibrations into electrical energy. They are the main candidates for supplying abandoned autonomous sensors in transport and industrial machines. Numerous practical implementations have been made recently [1]–[7], although most of these convert only a small part of the available mechanical energy (under 10%) [8]. This means that the interaction (also known as coupling) between the mechanical resonator and the conditioning electronics is weak. This suggests that the designers' effort should be focused on the optimization of the electromechanical conversion, considering the resonator, electrostatic transducer, and conditioning circuit as a whole [6], [9]–[13].

A VEH efficiency close to the theoretical limit is only reachable if the VEH is designed to operate in the mode of strong electromechanical coupling. The strong electromechanical coupling operation of VEH takes place when the energy converted by the electromechanical transducer is comparable with the energy related to the mechanical vibrations of the resonator (elastic and kinetic energies). In this mode, the resonator's mechanical behavior impacts strongly on the operation of the electronics connected to the transducer and vice versa: The electrical and mechanical domain operations can no longer be considered separately.

In the existing literature, the theoretical investigation of VEH operation in strong coupling mode has mainly been carried out for piezoelectric [14], [15] and electromagnetic [16] VEHs and for particular configurations of capacitive VEHs [12], [17]. Most of these studies are based on the hypothesis of a quasi-linear model of the electromechanical transducer. This paper proposes a general theoretical and analytical framework, allowing the description of VEH operation in the mode of strong electromechanical coupling, without any hypothesis about the linearity of operation and valid for VEHs with any kind of electromechanical transducers.

B. Consequences of Strong Electromechanical Coupling

For a harvester composed of a second-order lossless resonator and an electromechanical transducer of any nature, the absolute upper limit of the power that can be extracted, i.e., converted from the mechanical to electrical domain, is given by [18]

$$P_{h\,\max} = \frac{1}{2} A_{\text{ext}} \omega m X_{\max} \tag{1}$$

where $X_{\max}$ is the maximum allowed displacement of the resonator mobile mass, m is the resonator lumped mass, and ω and A_{ext} are the angular frequency and the acceleration amplitude of the external vibrations, respectively. The difficulties related with strong electromechanical coupling analysis can be illustrated on the example of a capacitive VEH. If the resonator is connected with a capacitive transducer operating in a triangular constant-charge QU (charge-voltage) cycle [11], the theoretical converted power is given by the well-known equation [19]

$$P_{h\,\text{converted}} = \frac{1}{2} U_0^2 C_{\max} \left(\frac{C_{\max}}{C_{\min}} - 1 \right) \frac{\omega_e}{2\pi} \tag{2}$$

Manuscript received March 02, 2010; revised June 13, 2010; accepted July 08, 2010. Date of publication November 11, 2010; date of current version January 28, 2011. This work was supported by the French National Agency of Research (ANR). This paper was recommended by Associate Editor M. Ortmanns.

D. Galayko is with the Laboratoire d'Informatique de Paris 6, Université Pierre et Marie Curie—Paris 6 (UPMC), 75252 Paris Cedex 05, France (e-mail: dimitri.galayko@lip6.fr).

P. Basset is with the ESYCOM Lab, ESIEE Paris, Université Paris-Est, 93162 Noisy-le-Grand Cedex, France (e-mail: p.basset@esiee.fr).

Digital Object Identifier 10.1109/TCSI.2010.2072030

where U_0 is the voltage across the transducer's electrical terminal when its capacity is maximal and ω_e is the angular frequency of variations of the transducer capacitance. ω_e can be different from ω if the capacity–displacement relation of the transducer is nonmonotonic [20]. $C_{\max}$ and $C_{\min}$ are the maximal and minimal values of the transducer's capacitance over one period of the mobile-mass vibration. They depend on the amplitude of the resonator vibrations and on the transducer's geometry.

For a given capacitive VEH, the value of the converted power expressed by (2) should be lower than the value given by (1). However, if U_0 is increased, from (2), it follows that the value of $P_{h\,\mathrm{converted}}$ is unbounded and can be greater than $P_{h\,\max}$. This apparent contradiction is explained by the fact that (2) is obtained under a hypothesis where the values of $C_{\max}$ and $C_{\min}$ are *known* and U_0-independent. This is true for low values of U_0, where the electromechanical coupling is weak and the force generated by the transducer on the resonator is negligible. If the value of U_0 is high, this hypothesis no longer holds: In VEH, $C_{\max}$ and $C_{\min}$ are related with the vibration amplitude of the mobile mass, and at high voltages of the transducer, the vibration amplitude is significantly affected by the force generated by the strongly biased electrostatic transducer. Hence, increasing U_0 modifies the mass vibration amplitude and, consequently, $C_{\max}$ and $C_{\min}$ so that the inequality $P_{h\,\mathrm{converted}} \leq P_{h\,\max}$ always holds.

So far, there has been no general technique to predict the mobile-mass vibration amplitude in such cases of strong electromechanical coupling and, hence, the level of converted power. The theory developed in this paper allows this prediction, making possible an optimal design of VEHs.

C. Analysis Techniques of Electromechanical Energy Conversion

In energy harvesting applications, the electromechanical transducers often operate in large-signal mode, which implies a strongly nonlinear behavior. There are two origins of nonlinearities. The first is related to the nonlinear mathematical relation between the dynamic quantities of transducers (force, voltage, strain, magnetic flux, displacement, etc.). In some cases, these nonlinearities are smooth and can be neglected, allowing analysis using a quasi-linear model [21], [22]. The second source of nonlinearity is the possible switching and nonlinear nature of the conditioning circuit operation. Even in the simple harvesting scheme of piezoelectric harvesters including a diode bridge and an output capacitive reservoir [15], the voltage applied across the electrical terminal of the transducer is a piecewise-defined wave. Here, the network topology connected to the transducer changes four times over one vibration period because of the switching behavior of the diode bridge. Electrostatic transducers behave nonlinearly in most cases because of the switching nonlinear conditioning circuits required by the energy conversion principle [23].

A common technique used to analyze the harvester operation consists in representing the transducer by its equivalent linear electrical model and connecting this model to the electrical schematic of the conditioning circuit. Such a system can be analyzed with the methods of electrical network analysis. However, this approach works only for cases where the nonlinearities of the transducer are smooth and, more importantly, when the equivalent electrical model of the transducer does not change with time. Typically, this is the case of harvesters using a piezoelectric or electromagnetic electromechanical interface [18], [24], [25]. The operation of an electrostatic transducer is more complex: Its equivalent electrical model is strongly nonlinear and time variant. For example, even for the simplest harvesting scheme based on a constant-charge triangular QU cycle [11], the electrical charge of the transducer capacitance and the generated force depend in a discontinuous way on the sign of the time derivative of the transducer capacitance (cf. Section IV-A). However, linearization of electrostatic transducers is still the dominant approach in the published studies: The capacitive transducer is often modeled as a spring [6], [26] or as a damper [18], [27]. These representations are locally correct on some time intervals of the transducer operation, but do not adequately model the global operation of the system.

The electromechanical coupling phenomena have been relatively well addressed in works dealing with piezoelectric or electromagnetic transducers. However, most of the studies of electrostatic transducers are focused on the conditioning circuit operation or on the design/optimization of the resonator+transducer block, with only a few considering the coupled operation of both [7], [13], [24]. Our work highlights that the operation mode and the topology of the conditioning electronics are just as important as the geometry of the transducer for the performance of the overall system. The theory proposed in this paper provides a general, simple, and rigorous tool which allows the understanding and the quantitative description of the interaction between the conditioning circuit, the resonator, and the transducer.

In this paper, we shall use the following naming conventions.

- Small letters shall denote the instantaneous real values of dynamic quantities, e.g., f for force, v for the velocity, and q for electrical charge.
- Capital letters shall denote the amplitude of sinusoidal quantities, e.g., F and V.
- Dotted capital letters shall denote the complex amplitudes of sinusoidal quantities, e.g., $\dot{F}$ and $\dot{V}$.
- Instantaneous voltages, currents, and capacitances shall be denoted by capital U, I, and C, respectively.

II. Analytical Model of Harvester

A. Description of the System

Harvesting of mechanical energy is achieved in two stages. First, a part of the mechanical energy of external vibrations is captured by the mechanical part of the harvester, which is, in most cases, composed of a mechanical resonator. Then, the electromechanical transducer achieves the transformation of this mechanical energy into an electrical form. The main role of the conditioning circuit is to create an electrical context needed for a proper operation of the electromechanical transducer.

Fig. 1 shows a general model for a mechanical energy harvester. In the mechanical domain, there are two reference frames: the global inertial frame Oy, in which the external vibrations take place with acceleration a_{ext}, and the reference

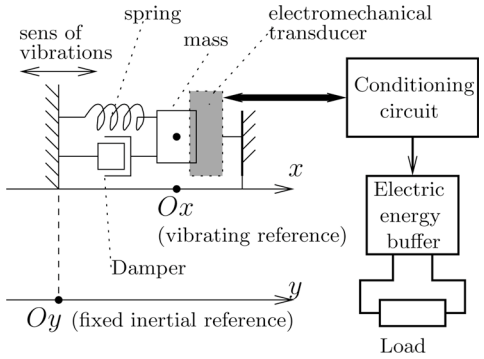

Fig. 1. General VEH diagram.

TABLE I
SUMMARY OF EQUIVALENCE BETWEEN MECHANICAL AND ELECTRICAL QUANTITIES

Mechanical quantity	Electrical quantity
Force, f	Electromotive force, $\mathcal{E}$, equal to minus voltage, $-u$.
Velocity, v	Current, i
Position, x	Charge, q
Mass, m	Inductance, L
Stiffness, k	Reciprocal of capacitance, $1/C$
Damping coefficient μ	Resistance, R

frame Ox related to the vibrating system in which the harvester is located. Usually, the motion of the Ox reference frame is modeled by applying a force $-ma_{\text{ext}}$ to the resonator (m is the resonator's mass), and then, the Ox reference frame is considered as inertial [28]. The resonator can be modeled with its lumped-parameter model composed of a mass (m), an elastic spring (with stiffness k), and a viscous damper (with damping coefficient μ). The electromechanical transducer is a device having two mechanical terminals: One is fixed with respect to the Ox reference frame, and the second is attached to the moving mass. The transducer generates a force f_t on the mass, and this force depends on the distance between its terminals (thus, on the mass position in the Ox reference frame) and on the transducer's electrical state (voltage, current, etc.).

We suppose that the external acceleration is sinusoidal, with a known amplitude A_{ext} and an angular frequency ω, $\omega = 2\pi/T$, with T being the vibration period. The resonator is supposed to be narrow band, i.e., with a quality factor above 10, and ω is close to the resonator's resonance frequency.

The presented method is inspired by techniques used for the analysis of electrical networks; hence, we use the electromechanical equivalence for the representation of mechanical quantities (cf. Table I). The mechanical system in Fig. 1 is represented by the equivalent electrical network in Fig. 2.[1] The force $-ma_{\text{ext}}$ is represented by an independent voltage source. The transducer is represented by an electrical dipole whose voltage (the force) depends, generally, on the displacement and, thus, on the velocity (current). The mechanical resonator is equivalent to a series RLC network.

[1]Strictly speaking, two equivalent electromechanical analogy systems are possible because of the duality of the electrical networks [29]. This paper uses the equivalence definition in which the velocity is equivalent to the current.

f_t depends not only on the transducer's physical nature and geometry but also on the associated electrical dynamic quantities (voltage, charges, electrical or magnetic field, etc.). For this reason, the presented theory deals with a block "transducer + conditioning electronics," rather than with an isolated device interfacing electrical and mechanical systems. This is a very important point, which distinguishes this work from previously proposed approaches.

B. First-Harmonic Method

This section presents how the nonlinearity of the VEH can be dealt with through the use of the first-harmonic method.

If the external acceleration is periodic, it can be assumed that all mechanical quantities of the harvester are periodic as well. Although this is not exactly true on large timescales for complex conditioning circuits [3], where the electric parameters of the conditioning circuit change slowly in time, at a timescale of several vibration periods, f_t can be considered periodic. Here, f_t is not necessarily sinusoidal. For example, a quasi-linear piezoelectric transducer associated with a sinusoidally vibrating resonator generates a sinusoidal force if connected with a linear resistor, but the force is nonsinusoidal if the conditioning circuit includes a diode bridge and a reservoir capacitor in parallel with the load resistance [15]. The narrow-band hypothesis stated in Section II-A implies that if a resonator is excited with a nonsinusoidal periodic external force and if this force has the first (fundamental) harmonic inside the passband of the resonator, the upper harmonics of the force are attenuated by the resonator frequency response, and the oscillations of the resonator can be considered as sinusoidal at the fundamental frequency of the external excitation. In this case, the higher harmonics of the force can be neglected. This assumption is the base of the first-harmonic method, which is a simplified version of the harmonic balance method [30]. Our analysis is only valid for the cases where this assumption is valid, i.e., where the energy injected in the mechanical system by the fundamental harmonic of the nonlinear force is much greater than the energy injected by the higher harmonics (e.g., the former representing 90% of the overall energy injected by this force).

Fig. 3 shows the transducer as a nonlinear operator which receives a sinusoidal signal at the input (the transducer's mobile mechanical terminal displacement) and outputs a nonsinusoidal periodic force. Considering only the fundamental harmonic of the output quantity means representing the transducer by a model which reproduces a *summarized* contribution of the nonlinear properties of the transducer. This model is only characterized by a ratio between the amplitudes of the input and output quantities and by the phase shift, i.e., by a complex transmission coefficient which is redefined for each amplitude value of the input signal. In this sense, the equivalent model is not linear, but it can be dealt with as linear in the context in which the input amplitude is constant, i.e., in the analysis of the asymptotic (steady-state) behavior of the system. Hence, in the further analysis, the nonlinear element of the network in Fig. 2 is replaced with a dipole responding to a sinusoidal current (velocity) by a sinusoidal voltage (transducer's force): Such an element can be

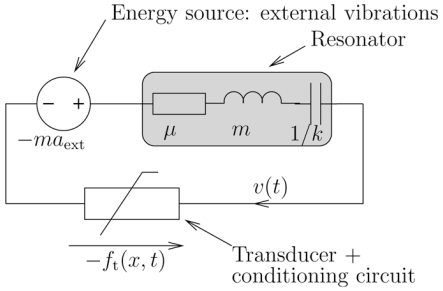

Fig. 2. Equivalent electrical representation of the harvester in the mechanical domain.

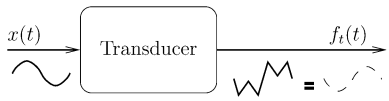

Fig. 3. Representation of nonlinear electromechanical transducer in the first-harmonic method.

characterized by a mechanical impedance, and the whole network can be analyzed as linear.

C. Mechanical Impedance of Nonlinear Transducer

Usually, an impedance is defined for linear electrical systems submitted to sinusoidal excitations. The mechanical impedance Ψ is defined equivalently to its electrical counterpart

$$\Psi = -\frac{\dot{F}}{\dot{V}} \tag{3}$$

where $\dot{F}$ and $\dot{V}$ are the complex amplitudes of the sinusoidal force and velocity of the point of force application, respectively. The complex amplitudes can be obtained by calculating the fundamental coefficients of the complex Fourier series.

As we said, f_t is generally nonsinusoidal. For this reason, the impedance definition of (3) is not applicable for the transducer and, in the context of the first-harmonic analysis, should be redefined as the ratio between minus the complex amplitude of the fundamental harmonic of f_t ($\dot{F}_t^{\omega}$) and the complex amplitude of the sinusoidal velocity of the moving terminal of the transducer

$$\Psi_t = -\frac{\dot{F}_t^{\omega}}{\dot{V}}. \tag{4}$$

Because of the nonlinear relation between the force and the resonator displacement, the mechanical transducer's impedance depends on the mobile terminal displacement amplitude.

The transducer's force f_t depends on the transducer's electrical state defined by the conditioning circuit. Hence, the definition of the mechanical impedance of a transducer can only be done for the whole system composed of the transducer and of the conditioning circuit with its specified operation mode. The operation mode can be characterized by a set of parameters which we call $\mathcal{P}$. The transducer's impedance is a complex-value function of these parameters.

Calculation of the transducer's mechanical impedance is quite complex even for simple harvesting systems and, in many cases, can only be obtained numerically. We propose the following general procedure, which is applicable to VEHs with any nature of electromechanical transducer. First, the value of the velocity amplitude V for which the transducer's impedance is calculated is fixed. The mobile electrode of the transducer is supposed to have a sinusoidal motion with velocity $v(t)$

$$v(t) = V\cos(\omega t + \phi_v) \tag{5}$$

where V and ϕ_v are the amplitude and the initial phase of the mobile terminal displacement. The value of ϕ_v does not matter in the impedance calculation and can be fixed arbitrarily. If the transducer and the conditioning circuit have internal energy states, they must be initially defined. These initial parameters of the conditioning circuit can be included in the vector $\mathcal{P}$.

Then, under this hypothesis of the mobile-mass displacement, the electrical quantities defining the transducer's force are calculated using the model of the transducer and of the conditioning circuit. From these quantities, the force f_t generated by the transducer on one mobile-mass vibration period is calculated. The mechanical impedance of the transducer is then calculated using (4), with $\dot{F}_t^{\omega}$ and $\dot{V}$ obtained as the fundamental coefficient of the complex Fourier series calculated for f_t and $v(t)$, respectively.

The calculation of f_t is the most complex step of this procedure. It depends on the system "transducer+conditioning circuit." In the case of piezoelectric VEHs, the transducer submitted to a deformation (strain) generates a current which, interacting with the conditioning circuit, results in some voltage on the piezoelectric transducer's electrodes. Hence, a mechanical force applied to the resonator is generated by the transducer. In the case of electromagnetic VEHs, the imposed displacement of a coil or magnet results in an induced electromotive force, which, interacting with the conditioning circuit, results in a current in the coil, which generates a force when interacting with the magnet. For electrostatic VEHs, the detailed description of the transducer's impedance calculation will be given in Section IV.

The next section demonstrates the practical use of the mechanical impedance definition in the analysis of mechanical energy harvesters.

III. Analysis of VEHs Through the Concept of Mechanical Impedance

A. Principle

The second Newtonian law written for the mobile mass is equivalent to the mesh equation for the network in Fig. 2. In steady-state harmonic mode, the complex amplitudes of the dynamic quantities are defined by

$$-m\dot{A}_{\text{ext}} = (\Psi_t + \Psi_r)\dot{V} \tag{6}$$

where Ψ_r is the mechanical impedance of the resonator given by

$$\Psi_r = \mu + \frac{k}{j\omega} + j\omega m \tag{7}$$

and $\dot{A}_{\text{ext}}$ is the complex amplitude of the external vibration's acceleration. This is a nonlinear equation, since $\dot{V}$ and Ψ_t both depend on V. The solution to the problem presented in Section I-B,

i.e., finding the mass displacement amplitude corresponding to a given $\mathcal{P}$ and to a given conditioning circuit, is simply found by equating the absolute values of both parts of (6)

$$mA_{\text{ext}} = |\Psi_t + \Psi_r| \cdot V. \tag{8}$$

This equation is algebraic and nonlinear and can have several solutions. The resolution of (8) requires a knowledge of the transducer impedance function $\Psi_t(V)$ which is found following the procedure described in Section II-C.

However, in the context of harvester design, the problem is inverse: how to find the operation mode of the conditioning circuit to ensure a given vibration amplitude defined by the resonator geometric constraints, whereby the maximal harvesting power can be achieved. For this case, (8) is rewritten

$$\frac{mA_{\text{ext}}}{V} = |\Psi_t + \Psi_r|. \tag{9}$$

If V is fixed, this equation uniquely defines the modulus of the total impedance of the system $\Psi_s = \Psi_r + \Psi_t(\mathcal{P})$. On an impedance chart, the corresponding locus is the circle $|\Psi_s| = (mA_{\text{ext}}/V)$. The set of solutions is given by the intersection of this circle with the locus $\Psi_r + \Psi_t(\mathcal{P})$ plotted on the same chart, when the components of the $\mathcal{P}$ vector vary in the allowed range. The solution set can contain zero, one, or many points, depending on the shape of the $\Psi_r+\Psi_t(\mathcal{P})$ locus. In the language of complex amplitudes, the real harvested power P is then given by [29]

$$P = \frac{1}{2}|\dot{V}|^2 \text{Re}\Psi_t = \frac{1}{2}V^2 \text{Re}\Psi_t. \tag{10}$$

Since V is fixed, among several possible solutions, the maximal harvested power corresponds to the solution point on the impedance chart for which $\text{Re}\Psi_t$ is maximal.

Equation (10) suggests that, to maximize the harvested power, both the amplitude V and the real part of the transducer's impedance are to be maximized. Indeed, this is true in most practical cases. However, as we said before, V and $\text{Re}\Psi_t$ are not mathematically independent, and in principle, there can exist a configuration of VEHs in which, at least for some range of V values, the harvested power is higher for smaller amplitudes.

B. Stability of Solutions

The aforementioned analysis allows one to find the asymptotic solutions of oscillator equations, but it does not guarantee that the obtained solutions are stable. The problem of instability can be illustrated as follows. In a harvesting system, the transducer mechanical impedance depends on the mobile-mass vibration velocity amplitude, i.e., $\Psi_t = \Psi_t(V)$. The transducer is mechanically connected to a resonator having an impedance Ψ_r. Hence, the total complex mechanical load impeding to the external force $-m\dot{A}_{\text{ext}}$ has an impedance $\Psi_s(V) = \Psi_r + \Psi_t(V)$. Let us assume that the system behaves following an asymptotic solution with velocity amplitude V_0 and that there is a perturbation (for example, an irregularity on the external vibration acceleration function) such that the velocity amplitude increases by ΔV and temporarily becomes $V_1 = V_0 + \Delta V$. After the end of the perturbation, a stable system comes back to the asymptotic solution with the amplitude V_0 after some time, whereas an unstable system goes away from this solution and comes to another stable solution or diverges. This is the definition of the amplitude stability we use for our system. On the basis of this definition, here, we present the derivation of a necessary and sufficient amplitude stability criterion for an asymptotic solution.

To find the necessary criterion, we suppose that the studied system is stable according to the aforementioned amplitude stability definition and remains in the steady state corresponding to the amplitude V_0. If, immediately after the end of a small perturbation, the system has the vibration amplitude $V_1 = V_0+\Delta V$, at this moment, the total mechanical impedance of the system Ψ_s equals to $\Psi_1 = \Psi_s(V_0+\Delta V)$. From (8) to this impedance value and to the external force, $-m\dot{A}_{\text{ext}}$ corresponds to an asymptotic vibration amplitude V_1'

$$V_1' = \frac{mA_{\text{ext}}}{|\Psi_1|}. \tag{11}$$

If $V_1 \neq V_1'$, the system cannot remain in the perturbed state with the amplitude V_1 and tends to adjust its amplitude to V_1'.[2] It means that the amplitude changes *in the direction of* V_1'. We note that V_1' is not the actual (new) stable state: When the system changes the amplitude in the direction of V_1', the transducer's impedance changes and the "target" amplitude of the system is not V_1' anymore. However, the position of V_1' is important, since it defines the dynamics of the system after the perturbation: If the amplitude V_0 is closer to V_1' than to V_1, after the perturbation, the amplitude tends toward V_1', asymptotically approaching the initial unperturbed state V_0. This happens if the system is stable, since in this case, the system's dynamics reduces the perturbation. Mathematically, this necessary stability condition can be expressed in the following way:

$$|V_0 - V_1'| < |V_0 - V_1| = |\Delta V|. \tag{12}$$

Given $V_1' = (mA_{ext}/|\Psi(V_0 + \Delta V)|)$ and $V_0 = (mA_{ext}/|\Psi(V_0)|)$, we have

$$mA_{\text{ext}} \frac{\left|\frac{1}{|\Psi(V_0+\Delta V)|} - \frac{1}{|\Psi(V_0)|}\right|}{|\Delta V|} < 1 \tag{13}$$

or if $|\Delta V| \to 0$

$$mA_{\text{ext}} \left|\frac{d}{dV}\frac{1}{|\Psi(V)|}\right| < 1\Bigg|_{V=V_0}. \tag{14}$$

Given that, from (6), $mA_{\text{ext}} = (V_0/|\Psi(V_0)|)$, we have

$$\left|\frac{d\,|\Psi(V)|}{dV}\Bigg|_{V=V_0}\right| < \left|\frac{\Psi(V_0)}{V_0}\right|. \tag{15}$$

The last equation provides a simple necessary stability criterion for a given solution. It is also a sufficient criterion: To prove it, it is enough to prove the contraposition, i.e., to show through

[2]If not, it means that, in the vicinity of V_0, there is an infinite set of solutions for (8). Such a case is not practical and is not considered here. For this demonstration, we suppose that the set of equation (8) roots is countable (so is for the set of steady states of the VEH), and moreover, the roots are spaced by a finite distance.

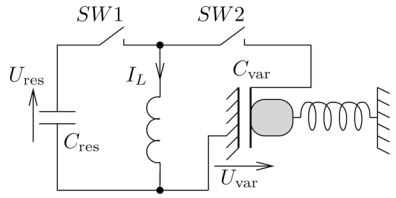

Fig. 4. Conditioning circuit for electrostatic transducer implementing a charge-constant energy conversion (Fig. 5) [11].

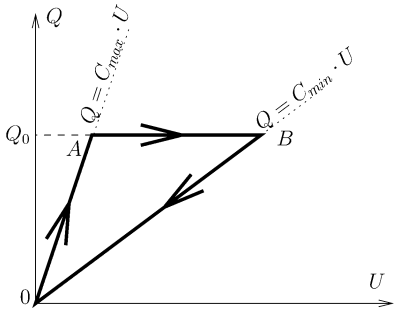

Fig. 5. QU cycle corresponding to the constant-charge energy conversion with electrostatic transducer.

the same reasoning that, for the unstable solution of (8), the inequality (15) has the opposite sign. It is interesting to note that this stability criterion is defined for a given velocity amplitude V_0, value of $\mathcal{P}$, and angular frequency and does not depend on the amplitude of the external force. If the system mechanical impedance and its evolution through V is known, the relation (15) provides the information about the unstable amplitude set in which the system cannot remain at the given frequency.

IV. Study of Three VEH's Geometries Using Electrostatic Conversion

In this section, we apply the presented analysis method to the most simple and well-known electrostatic harvesting scheme using a triangular constant-charge QU cycle (Fig. 5) [11]. This configuration will be studied with three transducers having different $C_{\text{var}}(x)$ characteristics.

A. Presentation of the System

The simplest charge-constant electrostatic harvester is composed of a reservoir capacitor C_{res} precharged to some initial voltage U_{res}, a resonator/transducer device with variable transducer capacitance C_{var}, an inductor, and two switches (Fig. 4). The inductor is used as an energy buffer for lossless energy exchange between C_{var} and C_{res}.[3] The circuit operates in the following way [19]. In the initial state (point O), the transducer capacitance is maximal and C_{var} is discharged. At this moment, the switch $SW1$ becomes ON, $SW2$ becomes OFF, and the inductor is charged by the capacitor C_{res} so that its current I_L increases to some value I. Then, $SW1$ becomes OFF, $SW2$ becomes ON, and the energy of the inductor is transferred to C_{var}, charging it to some charge Q_0. This process corresponds to the line OA and is supposed to be very fast, compared with the period of the C_{var} variation. Then, the switches are OFF and the transducer capacitances decrease, increasing the voltage and the energy of C_{var} (line AB). When C_{var} is minimal, its energy is quickly transferred to C_{res} using again the inductor as an energy buffer (line BO). Then, the transducer's capacitor is discharged and C_{var} increases until $C_{\max}$ again, returning the circuit in the initial point of the cycle.

The initial charge Q_0 defines the initial C_{var} voltage U_0 as $U_0 = Q_0 C_{\max}$ and is the key parameter for the energy yield of the harvester, as indicated in (2). Q_0 is defined by the maximal value of the inductor current I and by the maximal value of the transducer capacitor on the vibration cycle, with the latter depending on the resonator vibration amplitude. Thus, from the equality of energies $LI^2/2 = Q_0^2/(2C_{\max})$, Q_0 is given by

$$Q_0 = I\sqrt{C_{\max} L}. \tag{16}$$

In this demonstration, we consider I as a free design parameter whose choice must optimize the operation of the system (e.g., must maximize the energy yield). Supposing that C_{res} is large and its voltage U_{res} is nearly constant, I is determined as

$$I = \int_0^{\Delta t} \frac{U_{\text{res}}}{L} \mathrm{d}t = \frac{U_{\text{res}}}{L} \Delta t \tag{17}$$

where Δt is the time interval during which the switch $SW1$ is on. The value of I is fixed by the appropriate choice of Δt.

In the next sections, we shall present the analysis with three transducers having different $C_{\text{var}}(x)$ characteristics along the mobile-mass trajectory: linear, triangular, and hyperbolic (Fig. 6). The vector $\mathcal{P}$ of design parameters introduced in Section II-C includes only I. For the three cases, we calculate the mechanical impedance of the transducer/conditioning circuit block as a function of the operation parameter I. We fix the following design objective: to determine the appropriate value of I such that the mass vibration amplitude fits with the maximum value given by the transducer geometry. Apart from I, all parameters of the harvester are known and fixed and are given in Table II. We intentionally choose the transducer's characteristics $C_{\text{var}}(x)$ such that they have the same $C_{\max}$ and $C_{\min}$ at the desired mass vibration amplitude $X_d = 50$ μm. This will allow us to highlight the behavior differences due to the various shapes of the $C_{\text{var}}(x)$ characteristics.

The three studied configurations operate in the mode of strong electromechanical coupling. Indeed, without a transducer or with a deactivated conditioning circuit, the amplitude of the resonator vibration is 68 μm (can be obtained using the values of Table II and the (9) with $\Psi_t = 0$). Hence, with the value of I corresponding to the design objective, the presence of the transducer and conditioning circuit has to decrease the mass vibration amplitude to $X_d = 50$ μm, i.e., by 26%.

B. Area-Overlap Transducer

In the simplest case, $C_{\text{var}}(x)$ is linear, which corresponds to the in-plane moving transducer with variable electrode overlap area. This is typically the case for transducers having a comb-drive geometry [31]

$$C_{\text{var}}(x) = C_0 + \alpha x \tag{18}$$

[3]Without an inductor, an energy exchange between two capacitors always implies losses.

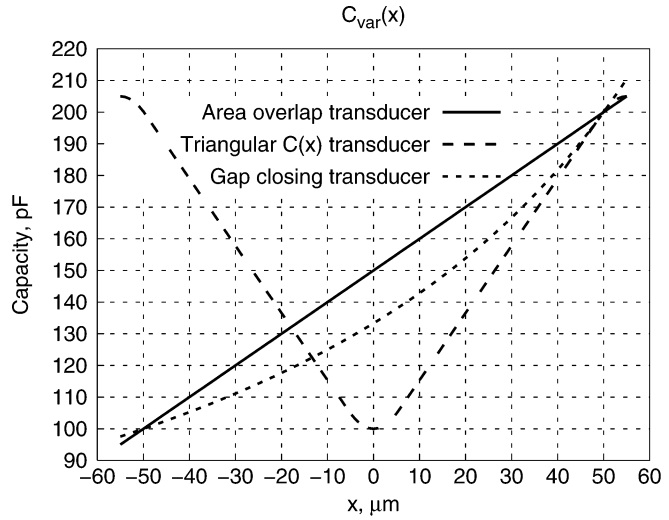

Fig. 6. $C_{\rm var}(x)$ characteristics of the capacitive transducers used in this study.

TABLE II
PARAMETERS OF THE MODELED SYSTEM

Mass, kg	m	$50 \cdot 10^{-6}$
Stiffness, Nm^{-1}	k	150
Quality factor, Nm^{-1}	Q	40
Damping factor, Nsm^{-1}	μ	$2.16{\cdot}10^{-3}$
Natural resonance frequency, Hz		275.7
External vibration frequency, Hz	$\omega/(2\pi)$	285
External vibration acceleration, ms^{-2}	A_{ext}	15
Buffer inductance, H	L	3e-3
Desired mobile mass vibration amplitude, μm	X_d	50
Maximal transducer capacitance corresponding to amplitude X_d (fig. 6), pF	C_{max}	200
Minimal transducer capacitance corresponding to amplitude X_d (fig. 6), pF	C_{min}	100

where C_0 and α are constant positive parameters depending on the transducer's dimensions. In Fig. 6, $C_0 = 150$ pF and $\alpha = 10^{-6}\ Fm^{-1}$.

1) Mechanical Impedance of Area-Overlap Transducer: The voltage on $C_{\rm var}$ can be easily expressed considering cosinusoidal motion of the mobile electrode, with the initial phase chosen at zero

$$x = X_d \cos \omega t. \tag{19}$$

The voltage across $C_{\rm var}$ is nonzero only when its capacitance decreases. Hence, we have

$$U_{\rm var}(t) = \frac{q_{\rm var}(t)}{C_{\rm var}\left(x(t)\right)} = \begin{cases} \frac{Q_0}{C_0 + \alpha X_d \cos \omega t}, & 0 < t \le \frac{T}{2} \\ 0, & \frac{T}{2} < t < T. \end{cases} \tag{20}$$

Here, we suppose that the charge/discharge of the variable capacitor are instantaneous.

For the transducer force, we have

$$f_t(t) = \frac{U_{\rm var}^2}{2}\frac{dC_{\rm var}}{dx} \tag{21}$$

$$= \begin{cases} \frac{0.5 Q_0^2 \frac{\alpha}{C_0^2}}{\left(1 + \frac{\alpha X_d}{C_0}\cos \omega t\right)^2}, & 0 < t \le \frac{T}{2} \\ 0, & \frac{T}{2} < t < T. \end{cases} \tag{22}$$

The first coefficient of the complex Fourier series of $f_t(t)$ is given by

$$\dot{F}_t^{\omega} = \frac{\omega}{\pi}\int_0^T f_t(t) e^{-j\omega t} dt. \tag{23}$$

A closed form of this integral can be found if the real and imaginary parts are calculated separately. We obtain

$$\dot{F}_t^{\omega} = \frac{1}{2} Q_0^2 \frac{\alpha}{C_0^2}\left(-\frac{a}{(1-a^2)^{\frac{3}{2}}} - j\frac{2}{\pi(1-a^2)}\right) \tag{24}$$

where $a = \alpha X_d / C_0$.

From (16) and given $C_{\max} = C_0 + \alpha X_d$, we have

$$Q_0 = I\sqrt{C_0 L}(1+a)^{0.5} \tag{25}$$

$$\dot{F}_t^{\omega} = \frac{1}{2} I^2 L \frac{\alpha}{C_0}\left(-\frac{a}{(1-a)\sqrt{1-a^2}} - j\frac{2}{\pi(1-a)}\right). \tag{26}$$

The complex amplitude of velocity is given by

$$\dot{V} = \omega \dot{X} = j\omega X_d = j\omega a C_0/\alpha \tag{27}$$

since $\dot{X} = X_d$ from (19).

Thus, for the impedance, we have, from (4)

$$\Psi_t = \frac{1}{2\omega} I^2 L \frac{\alpha^2}{C_0^2}\left(\frac{2}{\pi a(1-a)} - j\frac{1}{(1-a)\sqrt{1-a^2}}\right). \tag{28}$$

The total mechanical impedance is complex and depends on the vibration amplitude (represented by a). The transducer can be modeled by a linear damper and a linear spring with positive stiffness: Indeed, the mechanical impedance of a linear damper is positive and real, and the mechanical impedance of a spring is of form $k_s/(j\omega)$, where k_s is the spring stiffness.

It is interesting to highlight the link between the transducer's impedance and the mechanical power calculated by (10) and (2). From the mechanical point of view, with (10), we have for the real power

$$P = \mathrm{Re}\Psi_t \cdot (X_d \omega)^2 = L I^2 \frac{\alpha^2}{C_0^2}\frac{X_d^2}{a(1-a)} \cdot \frac{\omega}{2\pi}. \tag{29}$$

Submitting, in (29), the relations between α, C_0, X_d, a, $C_{\max}$, and $C_{\min}$ valid for an area-overlap transducer described by (18), we exactly get (2). The expressions for the power given by (2) and (10) obtained from the consideration of mechanical and electrical behaviors, respectively, give exactly the same results. This suggests that our theory is consistent.

A nonzero imaginary part of the transducer's mechanical impedance explains the phenomenon of the resonance fre-

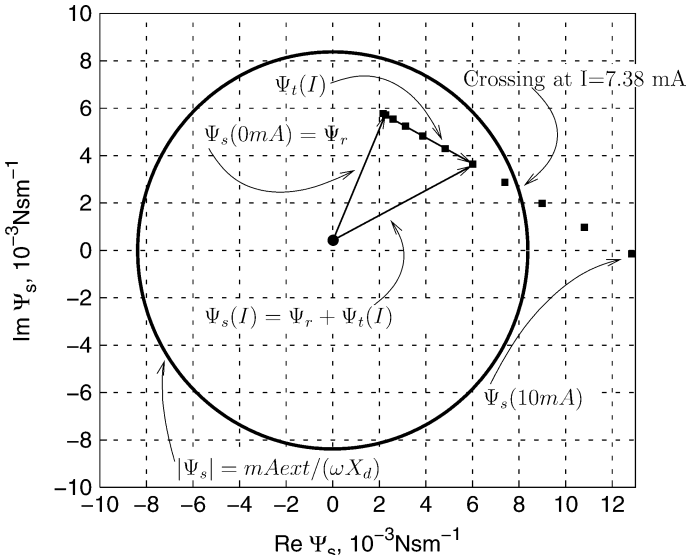

Fig. 7. Graphic resolution of (30) for area-overlap transducer. $\Psi_s(I)$ is plotted for $I = 1, 2, \ldots, 10$ mA.

quency shift of the resonator sometimes observed in practice [32]. Using the obtained mechanical impedance equation, it is possible to account for this shift and to design the harvester having a desired resonance frequency, or even to design a system able to adapt its resonance frequency to the frequency of external vibrations [33].

2) Calculation of the Charging Current I: Here, we show how to determine the current I needed to ensure the desired vibration amplitude X_d of the mobile mass. This is done using (9) which gives all possible values of I, allowing one to obtain the needed vibration amplitude X_d

$$|\Psi_t(X_d, I) + \Psi_r| = \frac{mA_{\text{ext}}}{\omega X_d}. \tag{30}$$

To solve (30), one can use a graphical method, as shown in Fig. 7. The horizontal and vertical axes represent the real and imaginary parts of mechanical impedance, respectively. On this chart, we plot the overall mechanical impedance of the system $\Psi_s = \Psi_t(X_d, I) + \Psi_r$ for the I current range that is expected to include the solution(s) (dots) and the locus corresponding to $|\Psi_s| = (mA_{\text{ext}}/\omega X_d)$ (plain line). The intersections between these two loci correspond to the values of I, ensuring the desired amplitude X_d. Among them, the optimal value of I corresponds to the rightmost point on the impedance chart. In this configuration, there is only one intersection point corresponding to $I = 7.38$ mA.

3) Validation of the Result: The aforementioned analysis of the harvester is validated by a behavioral modeling in the VHDL-AMS model [34]. This model had been previously validated with a tested electrostatic VEH [20], and for the present study, it was parameterized with the values presented in Table II and the calculated value of the current $I = 7.38$ mA. Running the simulation, we obtained the amplitude of 51 μm, as shown in the plot of the mobile-mass position (Fig. 8). The 2% difference from the aimed amplitude is explained by the fact that the dc component of the transducer's force was not accounted for. A 2.5-μm shift of the average mass position from zero is shown in Fig. 8. This modifies the C_{var} variation range compared with what was assumed in the analysis, producing a small modification of the solution of the mechanical equation.

This simulation suggests that the solution is stable, which can be checked with the stability criterion given by (15).

C. Transducer With Triangular $C_{\text{var}}(x)$ Characteristic

In this section, we apply the aforementioned analysis to a harvester having the same architecture and using the same mechanical resonator but employing a capacitive transducer exhibiting a triangular $C_{\text{var}}(x)$ characteristic (Fig. 6). All other parameters of the system are identical, except that in the model of the transducer where we added stoppers, limiting the vibration amplitude to ± 55 μm from the equilibrium position of the mobile mass. A transducer with a similar $C_{\text{var}}(x)$ shape was presented in [35].

1) Calculation of I and Validation: Given the complexity of $C_{\text{var}}(x)$, the mechanical impedance can only be calculated numerically. As for the case of the area-overlap transducer, we suppose that the mass displacement is given by (19). Thus, since the capacity $C_{\text{var}}(x)$ decreases from $C_{\max}$ to $C_{\min}$ during the first and third quarter periods, f_t is expressed with (31)

$$f_t(t) = \begin{cases} \frac{1}{2}\left(\frac{Q_0}{C_{\text{var}}}\right)^2 \frac{dC_{\text{var}}}{dx}, & 0 < \omega t < \frac{\pi}{2} \text{ or } \pi < \omega t < \frac{3\pi}{2} \\ 0, & \frac{\pi}{2} < \omega t < \pi \text{ or } \frac{3\pi}{2} < \omega t < 2\pi. \end{cases} \tag{31}$$

The first coefficient of the complex Fourier series $\dot{F}_t^{\omega}$ is found from the waveform of $f_t(t)$ and is used for Ψ_t calculation.

Fig. 9 shows the loci corresponding to $|\Psi_s| = mA_{\text{ext}}/(\omega X_d)$ and $\Psi_s = \Psi_t(X_d, I) + \Psi_r$, for $X_d = 50$ μm and for the same range of I as in Fig. 7. The intersection of these loci corresponds to $I = 3.10$ mA.

The modeling perfectly confirms this prediction. With $I = 3.10$ mA, after a transient process (Fig. 10), the mass vibration magnitude stabilizes at the value of 50 μm.

2) Case With Two Possible Solutions: In the two previous cases, the analysis resulted in a unique value of the current to achieve the desired vibration amplitude. However, in a different environment, (30) can provide two solutions, as shown by the

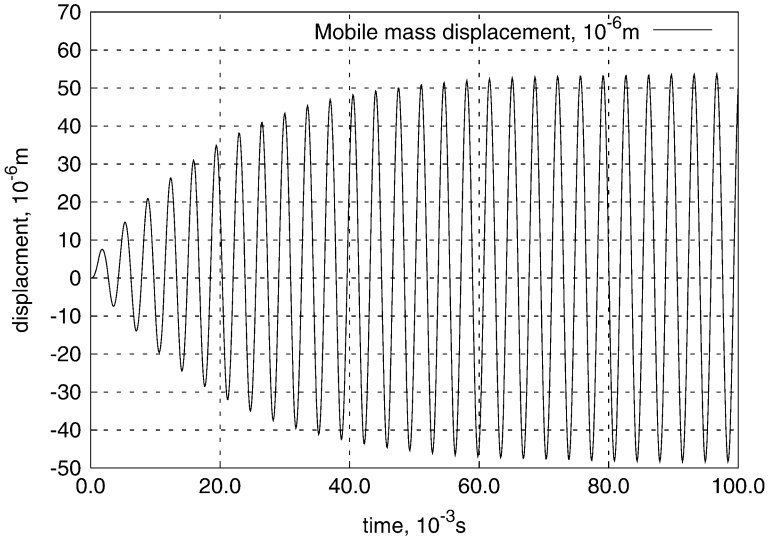

Fig. 8. Transient behavior of harvester with area-overlap transducer.

following example. If the same analysis is done, with an external vibration frequency $\omega/(2\pi)$ of 255 Hz instead of 285 Hz and with an external vibration amplitude A_{ext} of 21 ms^{-2} instead of 15 ms^{-2}, the resonator mechanical impedance Ψ_r is now at the semiplane corresponding to negative $\text{Im}\ \Psi_s$, close to the imaginary axis, and out of the circle $|\Psi_s| = mA_{\text{ext}}/(\omega X_d)$ (Fig. 11). As the transducer impedance is inversely proportional to the frequency, it does not change much when the frequency changes from 285 to 255 Hz. Thus, the Ψ_s locus is similar to that at a frequency of 285 Hz but is shifted so that, when $I = 0$, Ψ_s is equal to the new Ψ_r value. It can be seen that, now, there are two solution points, which means that the same displacement amplitude of 50 μm is obtained with $I = 2.1$ and 6.13 mA. The stability analysis indicates that these points are stable; thus, the designer has to choose between them. To optimize the converted power (10), the real part of the impedance must be maximized. Hence, among the two obtained values of I, the designer should choose the value giving the maximal real part of the impedance, i.e., corresponding to the rightmost solution point on the plot in Fig. 11.

D. Transducer With Hyperbolic $C_{\text{var}}(x)$ Function

In this section, we study a VEH with a very common transducer known as a gap-closing transducer. It corresponds to a parallel-plate capacitor, whose electrodes move in the axis perpendicular to the plane defining their surface. In this case, C_{var} is inversely proportional to the displacement

$$C_{\text{var}}(x) = \frac{C_0}{1 - \frac{x}{d}} \tag{32}$$

where C_0 and d are the C_{var} and the gap between the electrodes at $x = 0$, respectively.

We choose d and C_0 so that, at the desired displacement amplitude $X_d = 50$ μm, $C_{\max}$ and $C_{\min}$ are the same as those in the two previous cases

$$d = X_d \frac{C_{\max} + C_{\min}}{C_{\max} - C_{\min}} = 150 \cdot 10^{-6} \text{ m} \tag{33}$$

$$C_0 = C_{\max}\left(1 - \frac{X_d}{d}\right) = 133.3 \cdot 10^{-12} \text{ F}. \tag{34}$$

This case is the only configuration of electrostatic-based VEHs whose rigorous analysis can be found in literature [36].

1) Impedance Calculation: $C_{\text{var}}(x)$ is monotonic; thus, the system behaves exactly as in the case of the area-overlap transducer, except that the transducer's voltage U_{var} and force f_t are now equal to

$$U_{\text{var}}(t) = \frac{q_{\text{var}}}{C_{\text{var}}} = \begin{cases} \frac{Q_0}{C_0}\left(1 - \frac{X_d}{d}\cos\omega t\right), & 0 < t \le \frac{T}{2} \\ 0, & \frac{T}{2} < t < T \end{cases} \tag{35}$$

$$f_t(t) = \frac{U_{\text{var}}^2}{2}\frac{dC_{\text{var}}}{dx} \tag{36}$$

$$= \begin{cases} \frac{1}{2}\frac{Q_0^2}{C_0 d}, & 0 < t \le \frac{T}{2} \\ 0, & \frac{T}{2} < t < T. \end{cases} \tag{37}$$

Note that the expression of the force corresponds to the Coulombian damping force mentioned in [18] which is defined as $f_c(t) = F_0 \cdot \text{sign}(v(t))$, where F_0 is a constant and $v(t)$ is the velocity of the force application point. Hence, (37) defines a Coulombian damping force superposed to a constant bias force (cf. Section IV-D-3).

From (37), we obtain the first coefficient of the complex Fourier transform

$$\dot{F}_t^{\omega} = -j\frac{1}{\pi}\frac{Q_0^2}{C_0 d} \tag{38}$$

and from (4), at the desired amplitude X_s, the transducer's impedance is given by

$$\Psi_t = \frac{1}{\pi}\frac{Q_0^2}{C_0 d}\frac{1}{\omega X_d}. \tag{39}$$

Thus, a gap-closing variable capacitor, when used in the triangular constant-charge QU cycle, has a purely real impedance, i.e., it behaves like a viscous nonlinear damper.

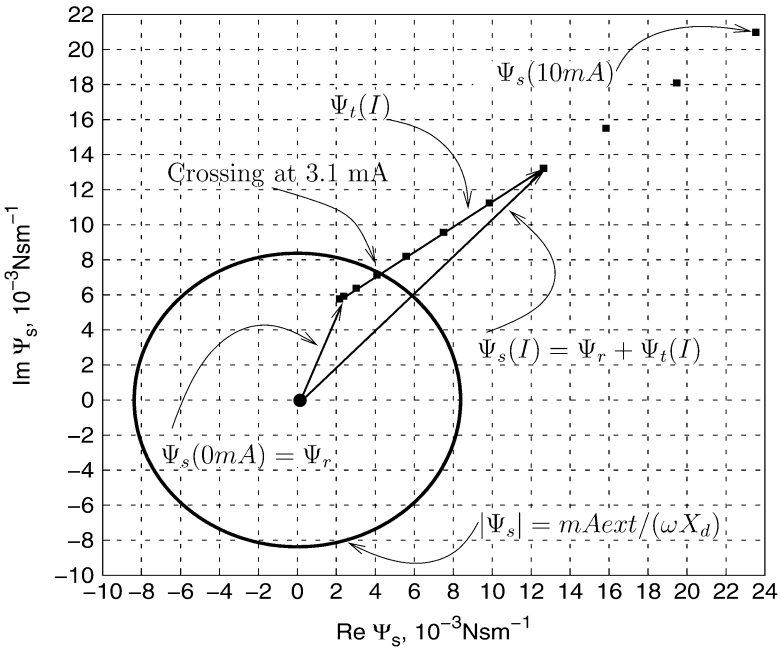

Fig. 9. Graphic resolution of (30) for the triangular $C_{\rm var}(x)$ characteristic transducer for the single-solution case. $\Psi_s(I)$ is plotted for $I = 1, 2, \ldots, 10$ mA.

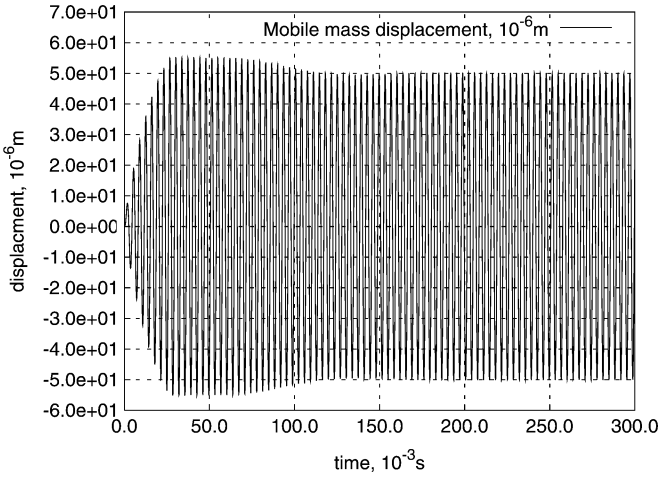

Fig. 10. Transient behavior of harvester with the triangular $C_{\rm var}(x)$ characteristic transducer.

2) Calculation of I: Varying the current I from 1 to 10 mA, we obtain the total mechanical impedance evolution $\Psi_s(I)$ given in Fig. 12. The unique current value yielding a vibration amplitude of 50 μm is 6.05 mA. This result is found analytically from (12) and (39) and is validated by behavioral modeling.

3) Comparison With Published Coulombian-Force Damped Harvesting Schemes: It is interesting to compare these results with the analysis done for the Coulombian-force damped resonator in [36] and reused in [18]. In this harvesting scheme, the force f_t generated by the transducer is always opposite to the velocity v of the mass motion and is equal to

$$f_t = -F_0 \cdot \mathrm{sign} v \tag{40}$$

where F_0 is a constant.

This case is very similar with our configuration. The only difference concerns the continuous (mean) component of f_t which is zero in (40) and is equal to half of the maximal force value in (37). However, since the system has a passband frequency response, this bias component can be neglected.

The analysis in [36] was carried out for a lossless second-order lumped-parameter mass–spring system excited by external sinusoidal vibrations through mechanical supports and submitted to a Coulombian damping force. The amplitude and the vibrations of the mass are calculated with regard to the resonator support (anchor). For the vibration amplitude, the following is obtained:

$$X^2/Y^2 = \omega_c^4 \left[\frac{1}{(\omega_c^2 - 1)^2} - \left(\frac{F}{mA_{\rm ext}\omega_c} \Gamma \right)^2 \right] \tag{41}$$

where X is the amplitude of the mass vibrations with regard to the resonator support, Y is the amplitude of the external vibrations, ω_c is the frequency of the external vibrations normalized to the natural resonance frequency ω_n of the mass–spring system ($\omega_c = \omega/\omega_n$), $A_{\rm ext}$ is the amplitude of the acceleration of the external vibrations, F is the absolute value of the Coulombian force, and Γ is given by

$$\Gamma = \frac{\sin(\pi/\omega_c)}{\cos(\pi/\omega_c) + 1}. \tag{42}$$

Unlike our model, in this analysis, the intrinsic damping coefficient of the transducer was considered zero, i.e., $\mu = 0$, and no hypothesis was made on the frequency of the resonator excitation (cf. Section II-A).

To compare this expression with what is predicted by our theory, we calculate X^2/Y^2 using the transducer's impedance. For this, we use (8), which gives the amplitude of the mass velocity. The mechanical impedance of the undamped resonator is given by

$$\Psi_r = j\omega m + k/(j\omega). \tag{43}$$

The Coulombian force generated by the gap-closing electrostatic transducer operating in the triangular charge-constant QU

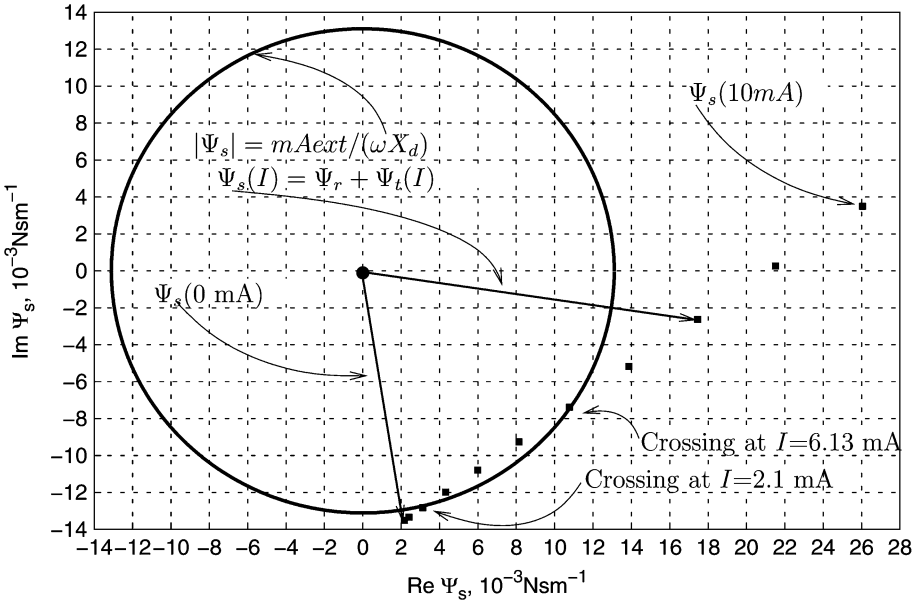

Fig. 11. Graphic resolution of (30) for the triangular $C_{\mathrm{var}}(x)$ characteristic transducer, for the case of two solutions. $\Psi_s(I)$ is plotted for $I = 1, 2, \ldots, 10$ mA.

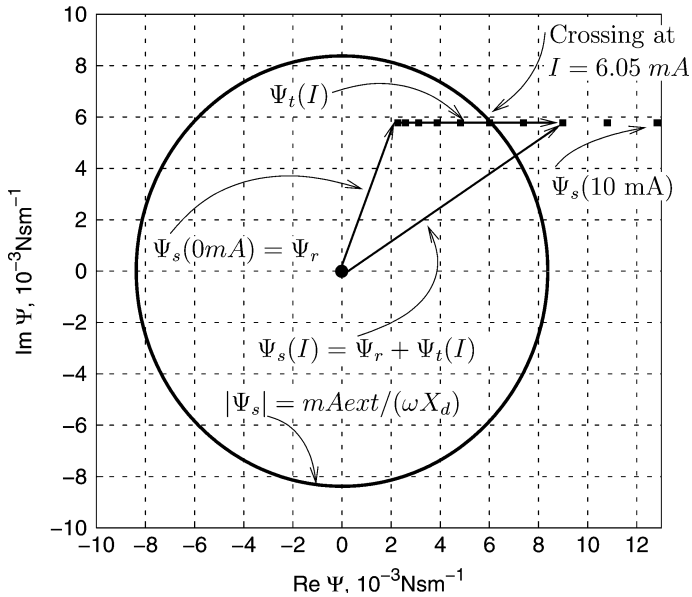

Fig. 12. Graphic resolution of (30) for the transducer with hyperbolic $C_{\mathrm{var}}(x)$. $\Psi_s(I)$ is plotted for $I = 1, 2, \ldots, 10$ mA.

cycle is half of the force it generates when the transducer's capacity decreases. Thus, from (37) and (40), we have

$$F = \frac{1}{4}\frac{Q_0^2}{C_0 d} \tag{44}$$

and from (39), the transducer's impedance is given by

$$\Psi_t = \frac{4}{\pi}\frac{F}{\omega X}. \tag{45}$$

From (8), (43), and (45), we have

$$V = \omega X = \frac{mA_{\mathrm{ext}}}{\sqrt{\left(m\omega - \frac{k}{\omega}\right)^2 + \left(\frac{4}{\pi}\frac{1}{\omega X}F\right)^2}}. \tag{46}$$

Taking $\omega = \omega_c\omega_n$, from this equation, we obtain

$$X^2 = \frac{(mA_{\mathrm{ext}})^2 - \left(\frac{4}{\pi}F\right)^2}{\omega_n^4 m^2\left((\omega_c^2 - 1)\right)^2}. \tag{47}$$

Given $Y = A_{\mathrm{ext}}/\omega^2 = (A_{\mathrm{ext}}/\omega_c^2\omega_n^2)$, we obtain

$$X^2/Y^2 = \omega_c^4\left[\frac{1}{(\omega_c^2 - 1)^2} - \left(\frac{\frac{4}{\pi}F}{mA_{\mathrm{ext}}\,(\omega_c^2 - 1)}\right)^2\right]. \tag{48}$$

To compare this with the Hartog's equation (41), we performed a limit development of the function $r(\omega_c) = 1/\Gamma(\omega_c)$ when $\omega_c \to 1$, i.e., when the frequency of the external vibration is near the resonance. We get

$$r(\omega_c) = 1/\Gamma(\omega_c) \approx \frac{\pi}{2}(\omega_c - 1). \tag{49}$$

From (41) and (49), we have

$$X^2/Y^2 = \omega_c^4\left[\frac{1}{(\omega_c^2 - 1)^2} - \left(\frac{\frac{2}{\pi}F}{mA_{\mathrm{ext}}\omega_c(\omega_c - 1)}\right)^2\right]. \tag{50}$$

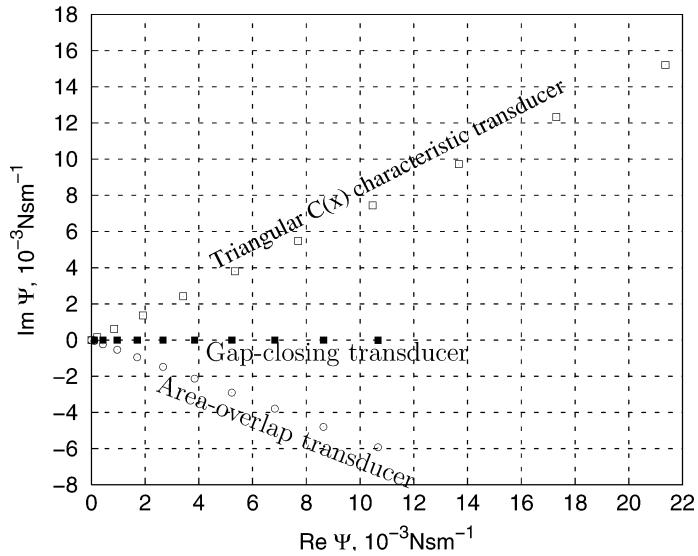

Fig. 13. Mechanical impedance of the transducers in the three studied cases against I. I changes from 0 to 10 mA, with 1-mA step.

Near resonance, $\omega_c \approx 1$ and the last equation is governed by $\omega_c - 1$ and $\omega_c + 1 \approx 2$: With this approximation, (50) is identical to (48). Hence, near resonance, our theory gives exactly the same result as the theory of Hartog, however, through a much simpler and more straightforward analytical development.

V. Discussions

Fig. 13 shows the evolution of the transducer's impedance over the I variation in the three studied cases. The differences in the impedance's plots come only from the differences in the shapes of $C_{\rm var}(x)$ curves, since all other operation parameters are identical in the three configurations (the amplitude and frequency of the mobile electrode displacement, $C_{\max}$ and $C_{\min}$, and, hence, Q_0 from (16) for each I). Considering the real parts of the impedances, we can see that, for each I, they are identical for the area-overlap and the gap-closing transducer, and the real part of the triangular $C_{\rm var}(x)$ characteristic transducer impedance is twice the corresponding values of the other two transducers. From (10), we may conclude that the corresponding values of the converted power are in the same relation. Equation (2) provides the same results: All the variables of this equation have the same values for the three cases except the frequency of $C_{\rm var}$ variation which is equal to the frequency of the mechanical vibration for the hyperbolic and area-overlap transducers and is twice this value for the triangular $C_{\rm var}(x)$ characteristic transducer. This similarity of results is to be expected, as (2) and (10) calculate the same quantity in different ways. Hence, for the considered harvesting scheme, the real part of the mechanical impedance of the capacitive transducer can be easily deduced from these two equations if $C_{\max}$, $C_{\min}$, Q_0, ω, and V are known. It does not depend on the shape of the $C_{\rm var}(x)$ characteristic, as long as the latter is monotonic, but only on the values of $C_{\rm var}(x)$ at the extreme positions of the mobile electrode.

However, the imaginary part of the impedance depends strongly on the shape of $C_{\rm var}(x)$. Let us consider the area-overlap and gap-closing transducers. In the first case, at $I = 10$ mA, the value of $\mathrm{Im}\Psi_t$ is $-0.006\ \mathrm{N \cdot s \cdot m^{-1}}$; in the second case, it is zero for all I (Fig. 13). However, the corresponding $C_{\rm var}(x)$ characteristics are numerically close: For each x, they differ by less than 10% (Fig. 6). Such sensitivity of the imaginary part of the mechanical impedance to the shape of $C_{\rm var}(x)$ is a very important result with significant impact on potential practical applications. The imaginary part of the impedance is responsible for the mechanical impedance matching between the transducer and the resonator and has a direct impact on the energy yield of the system. Moreover, not only the absolute value but also the sign of the imaginary part of the transducer's impedance is impacted by the $C_{\rm var}(x)$ shape. The sign of $\mathrm{Im}\Psi_t$ defines the direction of the shift of the system resonance frequency. This shift, being dependent on the electrical parameters of the conditioning circuit, means that an electrical tuning of the resonance frequency of the harvester can be achieved, allowing the broadening of the system bandwidth.

VI. Conclusion

This study has resulted in the development of a new analytical tool which enables one to address a large spectrum of practical issues related to the dynamic behavior of narrow-band VEHs. The mechanical impedance of a transducer is a universal criterion characterizing the efficiency of the power interface between the mechanical and the electrical domain. It is applicable to harvesters with any kind of electromechanical transducers and with any topology of conditioning circuit. For the first time, the relation between the shape of the transducer's characteristic $C_{\rm var}(x)$ and its mechanical impedance was highlighted and characterized.

The results of this study can be used to design the next generation of optimized conditioning circuits of VEHs, with the ability of smart behavior to dynamically adapt to variations of the external vibration parameters [37].

References

[1] E. O. Torres and G. A. Rincón-Mora, "Electrostatic energy-harvesting and battery-charging CMOS system prototype," *IEEE Trans. Circuits Syst.—I: Reg. Papers*, vol. 56, no. 9, pp. 1938–1948, Sep. 2009.

[2] P. Basset, D. Galayko, A. M. Paracha, F. Marty, A. Dudka, and T. Bourouina, "A batch-fabricated and electret-free silicon electrostatic vibration energy harvester," *J. Micromech. Microeng.*, vol. 19, no. 11, p. 115 025, Nov. 2009.
[3] B. C. Yen and J. H. Lang, "A variable-capacitance vibration-to-electric energy harvester," *IEEE Trans. Circuits Syst.—I: Reg. Papers*, vol. 53, no. 2, pp. 288–295, Feb. 2006.
[4] H. Lhermet, C. Condemine, M. Plissonier, R. Salot, P. Audebert, and M. Rosset, "Efficient power management circuit: Thermal energy harvesting to above-IC microbattery energy storage," in *Proc. ISSCC*, 2007, pp. 62–587.
[5] M. Marzencki, Y. Ammar, and S. Basrour, "Integrated power harvesting system including a MEMS generator and a power management circuit," *Sens. Actuators A, Phys.*, vol. 145/146, pp. 363–370, Jul./Aug. 2008.
[6] G. Despesse, T. Jager, J. J. Chaillout, J. M. Léger, A. Vassilev, S. Basrour, and B. Charlot, "Fabrication and characterization of high damping electrostatic micro devices for vibration energy scavenging," in *Proc. DTIP MEMS MOEMS Conf.*, 2005, pp. 386–390.
[7] S. Roundy and P. K. Wright, "A piezoelectric vibration based generator for wireless electronics," *Smart Mater. Struct.*, vol. 13, no. 5, pp. 1131–1142, Aug. 2004.
[8] P. D. Mitcheson, E. M. Yeatman, G. K. Rao, A. S. Holmes, and T. C. Green, "Energy harvesting from human and machine motion for wireless electronic devices," *Proc. IEEE*, vol. 96, no. 9, pp. 1457–1486, Sep. 2008.
[9] J. K. Ward and S. Behrens, "Adaptive learning algorithms for vibration energy harvesting," *Smart Mater. Struct.*, vol. 17, no. 3, p. 035 025, Apr. 2008.
[10] M. Lallart, L. Garbuio, L. Petit, C. Richard, and D. Guyomar, "Double synchronized switch harvesting (DSSH): A new energy harvesting scheme for efficient energy extraction," *IEEE Trans. Ultrason., Ferroelectr., Freq. Control*, vol. 55, no. 10, pp. 2119–2130, Oct. 2008.
[11] S. Meninger, J. O. Mur-Miranda, R. Amirtharajah, A. P. Chandrakasan, and J. H. Lang, "Vibration-to-electric energy conversion," *IEEE Trans. Very Large Scale Integr. (VLSI) Syst.*, vol. 9, no. 1, pp. 64–76, Feb. 2001.
[12] W. Ma, R. Zhu, L. Rufer, Y. Zohar, and M. Wong, "An integrated floating-electrode electric microgenerator," *J. Microelectromech. Syst.*, vol. 16, no. 1, pp. 29–37, Feb. 2007.
[13] G. K. Rao, P. D. Mitcheson, and T. C. Green, "Mixed electromechanical simulation of electrostatic microgenerator using custom-semiconductor device models," in *Proc. PowerMEMS Conf.*, Nov. 2009, pp. 356–359.
[14] Y. Liao and H. A. Sodano, "Model of a single mode energy harvester and properties for optimal power generation," *Smart Mater. Struct.*, vol. 17, no. 6, p. 065 026, Nov. 2008.
[15] Y. C. Shu and I. C. Lien, "Efficiency of energy conversion for a piezoelectric power harvesting system," *J. Micromech. Microeng.*, vol. 16, no. 11, pp. 2429–2438, Sep. 2006.
[16] S. P. Beeby, R. N. Torah, M. J. Tudor, P. Glynne-Jones, T. O'Donnell, C. R. Saha, and S. Roy, "A micro electromagnetic generator for vibration energy harvesting," *J. Micromech. Microeng.*, vol. 17, no. 7, p. 1257, Jun. 2007.
[17] G. G. Yaralioglu, A. S. Ergun, B. Bayram, E. Hzggstrom, and B. T. Khuri-Yakub, "Calculation and measurement of electromechanical coupling coefficient of capacitive micromachined ultrasonic transducers," *IEEE Trans. Ultrason., Ferroelectr., Freq. Control*, vol. 50, no. 4, pp. 449–456, Apr. 2003.
[18] P. D. Mitcheson, T. C. Green, E. M. Yeatman, and A. S. Holmes, "Architectures for vibration-driven micropower generators," *J. Microelectromech. Syst.*, vol. 13, no. 3, pp. 429–440, Jun. 2004.
[19] J. O. M. Miranda, "Electrostatic vibration-to-electric energy conversion," Ph.D. dissertation, MIT, Cambridge, MA, Feb. 2004.
[20] A. M. Paracha, P. Basset, D. Galayko, F. Marty, and T. Bourouina, "A silicon MEMS DC/DC converter for autonomous vibration-to-electrical energy scavenger," *IEEE Electron Device Lett.*, vol. 30, no. 5, pp. 481–483, May 2009.
[21] S. Roundy, "On the effectiveness of vibration-based energy harvesting," *J. Intell. Mater. Syst. Struct.*, vol. 16, no. 10, pp. 809–823, Oct. 2005.
[22] E. Halvorsen, "Energy harvesters driven by broadband random vibrations," *J. Microelectromech. Syst.*, vol. 17, no. 5, pp. 1061–1071, Oct. 2008.
[23] P. D. Mitcheson, T. Sterken, C. He, M. Kiziroglou, E. M. Yeatman, and R. Puers, "Electrostatic microgenerators," *Meas. Control J.—Lond. Inst. Meas. Control*, vol. 41, no. 4, p. 114, 2008.
[24] B. O. het Veld, D. Hohlfeld, and V. Pop, "Harvesting mechanical energy for ambient intelligent devices," *Inf. Syst. Frontier*, vol. 11, no. 1, pp. 7–18, Mar. 2009.
[25] J. L. Kauffman and G. A. Lesieutre, "A low-order model for the design of piezoelectric energy harvesting devices," *J. Intell. Mater. Syst. Struct.*, vol. 20, no. 5, pp. 495–504, Mar. 2009.
[26] Y. Chiu and V. F. G. Tseng, "A capacitive vibration-to-electricity energy converter with integrated mechanical switches," *J. Micromech. Microeng.*, vol. 18, no. 10, p. 104 004, Sep. 2008.
[27] M. S. M. Soliman, E. M. Abdel-Rahman, E. F. El-Saadany, and R. R. Mansour, "A wideband vibration-based energy harvester," *J. Micromech. Microeng.*, vol. 18, no. 11, p. 115 021, Oct. 2008.
[28] L. D. Landau and E. M. Lifshitz, *Course of Theoretical Physics: Mechanics*. Oxford, U.K.: Butterworth–Heinemann, 1976.
[29] I. Tskv, *Circuit Theory*. Noida, India: Tata McGraw-Hill, 1985.
[30] E. S. Levitan, "Forced oscillation of a spring–mass system having combined Coulomb and viscous damping," *J. Acoust. Soc. Amer.*, vol. 32, no. 10, pp. 1265–1269, Oct. 1960.
[31] W. C. Tang, T.-C. H. Nguyen, M. W. Judy, and R. T. Howe, "Electrostatic-comb drive of lateral polysilicon resonators," *Sens. Actuators A, Phys.*, vol. 21, no. 1–3, pp. 328–331, Feb. 1990.
[32] G. Despesse, "Etude des phénomènes physiques utilisables pour alimenter en énergie électrique des micro-systèmes communicants," Ph.D. dissertation, Institut National Polytechnique de Grenoble, Grenoble, France, 2005.
[33] J. J. Yao and N. C. MacDonald, "A micromachined single-crystal silicon tunable resonator," *J. Micromech. Microeng.*, vol. 5, no. 3, pp. 257–264, 1996.
[34] D. Galayko, R. Pizarro, B. Philippe, A. M. Paracha, and G. Amendola, "AMS modeling of controlled switch for design optimization of capacitive vibration energy harvester," in *Proc. Behav. Model. Simul. Conf.*, Sep. 2007, pp. 115–120.
[35] A. M. Paracha, P. Basset, P. Lim, F. Marty, and T. Bourouina, "A bulk silicon-based vibration-to-electric energy converter using an in-plane overlap plate (IPOP) mechanism," in *Proc. PowerMEMS*, 2006, pp. 169–172.
[36] J. P. Den Hartog, "Forced vibrations with combined Coulomb and viscous friction," *J. Appl. Mech.*, vol. 53, pp. 107–115, Dec. 1931.
[37] A. Dudka, D. Galayko, and P. Basset, "Smart adaptive power management in electrostatic harvester of vibration energy," in *Proc. PowerMEMS Conf.*, 2009, pp. 257–260.

Dimitri Galayko received the B.S. degree from Odessa National Polytechnic University, Odessa, Ukraine, in 1998, the M.S. degree from the National Institute of Applied Science in Lyon (INSA-LYON), Lyon, France, in 1999, and the Ph.D. degree from the University of Lille 1, Villeneuve d'Ascq, France, in 2002, where he made his Ph.D. thesis in the Institute for Electronics, Microelectronics and Nanotechnology (IEMN). The topic of his Ph.D. dissertation was the design of microelectromechanical silicon filters and resonators for radiocommunications.

Since 2005, he has been an Associate Professor with Université Pierre et Marie Curie—Paris 6 (UPMC), Paris, France, in the Laboratoire d'Informatique de Paris 6. His research interests include the design of integrated analog and mixed circuits and design of integrated interfaces with sensors.

Philippe Basset received the Engineering Diploma in electronics from the Institut Supérieur d'Electronique et du Numérique (ISEN), Lille, France, in 1997, and the M.Sc. and Ph.D. degrees from the Institute of Electronics, Microelectronics and Nanotechnology (IEMN), University of Lille 1, in 1999 and 2003, respectively.

In 2004, he was a Postdoc in Garry Fedder's group at Carnegie Mellon University, Pittsburgh, PA. In 2005, he joined ESIEE Paris, Université Paris-Est, Noisy-le-Grand, France, where he is currently an Associate Professor. His research interests are in the area of microelectromechanical systems (MEMS) sensors and actuators and micropower sources for autonomous MEMS.

Dr. Basset received a doctoral fellowship from the Centre National de la Recherche Scientifique for 2000–2003 and, in 2005, a three-year young researcher grant from the French Research Agency (ANR) to work on energy harvesting using micro- and nanotechnologies.